J Eng Math (2008) 61:55–68
DOI 10.1007/s10665-007-9174-2

On starting conditions for a submerged sink in a fluid

Lawrence K. Forbes · Graeme C. Hocking · Tim E. Stokes

Received: 12 July 2006 / Accepted: 11 July 2007 / Published online: 16 August 2007

Abstract Withdrawal of a fluid through an isolated line sink (for planar flow) or a point sink (for axi-symmetric flow in three dimensions) is considered. A linearized solution is presented in both cases, under the assumption that the sink strength is small and the sink is turned on gradually. The results show that the behaviour for small times is as if an image source were present above the surface. Asymptotic results indicate that, in both cases, the flow rapidly develops an effective image sink above the free surface.

Keywords Asymptotic behaviour · Heuristic derivation · Linearized solution · Method of stationary phase · Withdrawal flows

1 Introduction

The withdrawal of fluid from a tank, a reservoir or even the lens of fresh ground-water in an island is an important problem that has been much studied. Until relatively recently, theoretical modelling of these problems has mostly assumed steady flow conditions. This is because withdrawal is often a process that occurs on a long time-scale, so that the transients associated with start-up have long since ceased to be of interest. In addition, the computational modelling of a steady process is simpler, as it involves one fewer independent variable.

An important earlier contribution to the steady modelling of withdrawal flows was the paper of Tuck and Vanden-Broeck [1], who considered the canonically simple, but nonlinear, problem of a line sink beneath a free surface, in planar ideal flow. They showed that two types of flow configurations were possible. The first occurred over a range of small withdrawal rates and involved an almost horizontal free surface of the fluid, with a stagnation point directly above the sink. In the second flow type, the interface was drawn down into a vertical cusp above the sink. This second type occurred at only one particular value of the sink strength, and Hocking [2] presented an

L. K. Forbes (✉)
School of Mathematics and Physics, University of Tasmania, Hobart, TAS 7001, Australia
e-mail: larry.forbes@utas.edu.au

G. C. Hocking
Division of Science, School of Mathematics and Statistics, Murdoch University, Murdoch, WA 6150, Australia

T. E. Stokes
University of Waikato, Private Bag 3105, Hamilton, New Zealand

argument that it represented the critical withdrawal strength at which the interface would be drawn right down into the sink in a practical situation.

There is now a significant literature on this problem, much of which is focussed on attempting to resolve the relationship between the two solution types found by Tuck and Vanden-Broeck [1]. For planar flows, Forbes and Hocking [3] included surface tension and showed numerically that a fold bifurcation was present for the branch of solutions at small sink strength, near the maximum value. Steady withdrawal solutions have also been computed in three dimensions. Axi-symmetric free-surface flow into a submerged point sink was studied numerically by Forbes and Hocking [4] and later by Vanden-Broeck and Keller [5], and again it was found that there is a branch of steady solutions for small sink strength, with a limiting solution at some maximum strength. More complex flow configurations in fully three-dimensional flow have been computed by Forbes and Hocking [6] and in a similar problem in ground-water flow by Lucas and Kucera [7], for example.

It has become clear that a detailed understanding of the relationship between the steady solution types for withdrawal flows demands a consideration of the fully unsteady (time dependent) flow problem. For planar flow involving a submerged line sink, Tyvand [8] undertook a Taylor-series expansion to the second order in time. On the basis of this calculation, Tyvand then estimated a critical Froude number (sink strength) at which the interface might form a dip and be drawn downwards, although that calculation is possibly optimistic on the basis of such a low-order Taylor series. Sozer and Greenberg [9] used a model set of evolution equations to study the unsteady nonlinear development of planar withdrawal flows.

The time-dependent draining of a tank or reservoir has also been studied for three-dimensional fluid flow, with axially symmetric geometry. Zhou and Graebel [10] used a boundary-integral method to compute the evolution of the interface shape for draining flow from a circular tank, through a circular hole on the bottom at the centre. Their results show that the free surface forms a jet near the centre of the tank, and this may be directed either upwards or downwards, depending on the initial fluid depth and the radius of the drain hole. They suggested that the rapid formation of the jet may be related to the Rayleigh–Taylor instability. Very similar conclusions were reached by Baek and Chung [11] who included viscosity in a finite-difference approach. Xue and Yue [12] solved numerically for nonlinear axisymmetric flow caused by a submerged point sink in unbounded fluid, when the sink is turned on impulsively. They found three different flow behaviours, depending on the sink strength. For small strengths the interface eventually evolved to a steady-state (time independent) configuration, for moderate sink strengths an upward-directed jet formed, and for sufficiently strong sinks a downward jet was formed, drawing the free surface into the sink. Interestingly, these three different solution types were all formed for smaller sink strengths than the limiting strength at which Forbes and Hocking [4] computed their steady-state solutions. Such a striking difference in the limiting values of the Froude number (sink strength) may suggest that the likelihood of ever approaching a steady state in a time-dependent problem depends sensitively on the initial conditions for the flow, and hence its history.

Initial conditions have been the subject of recent discussion in the literature. The unsteady computations [10–12] discussed above evidently all started the solution from a horizontal initial free-surface profile, with an assumed zero velocity potential. These zero conditions were also adopted by Miloh and Tyvand [13] in a Taylor-series expansion of the axi-symmetric solution to third order in time. They estimated a critical sink strength at which dip formation at the free surface would occur; although their results are low-order only, they are not inconsistent with the full numerical results of Xue and Yue [12]. Imposing zero velocity potential on an initially flat interface is equivalent to placing an image source at an equal height above the surface to the depth of submergence of the sink below it.

By contrast, Stokes et al. [14] have investigated a range of different initial conditions for the flow, and used both Taylor-series expansion in time and a numerical semi-Lagrangian technique. They focussed on an initial condition which effectively has an image sink above the interface, rather than the image source of Miloh and Tyvand [13]. This is equivalent to establishing a steady-state flow beneath a rigid lid, and then impulsively removing the lid so that the free-surface position and the velocity potential may then evolve in time. Their numerical results suggested this gave behaviour similar to that which is obtained by gradually increasing the sink strength. It may be that this gentler method of starting the flow might allow steady-state situations to be achieved over a wider range of sink strengths, than is possible for the more extreme case in which the sink is turned on impulsively, so possibly

explaining the discrepancy between the results of Forbes and Hocking [4] and Xue and Yue [12]. Nevertheless, such initial conditions have been criticized by Tyvand and Haugen [15], who claim they would be impossible to produce due to the lack of tangential forces at the interface. This criticism cannot be true for situations such as those in which steady flows are first created beneath a rigid plane which is then impulsively removed, but might perhaps retain some validity in the extreme case in which the sink itself is turned on abruptly.

In the practical operation of a reservoir, the situation in which a sink in the fluid is turned on abruptly is unlikely to be of great interest. Rather, the sink strength varies smoothly, reflecting the changing demands on water during the day. The primary aim of the present paper, therefore, is to study the change in the analytical structure of the solution as a sink is turned on gradually; this is done here in the context of a linearized solution, valid for small sink strengths, since this enables detailed asymptotic study of the flow behaviour in a way that is not immediately available to fully nonlinear numerical techniques. Nevertheless, such a linearized analysis can only give information about the one behaviour type in which a steady-state solution is ultimately achieved. This fact was discussed by Xue and Yue [12], who identified this as an obvious weakness of purely linearized analyses. Their other two solution types, in which either upwardly or downwardly directed vertical jets are formed at the interface, are of course not accessible to this analysis. (These three behaviour types were also reported by Stokes et al. [14]). In Sect. 2, we summarize the heuristic arguments in favour of either the initial condition involving an image source above the fluid, employed by Tyvand [8], or the condition with an image sink, as discussed by Stokes et al. [14]. The linearized theory for two-dimensional (planar) flow into a line sink is then analyzed in detail in Sect. 3, and the corresponding calculations for the three-dimensional axisymmetric case of flow into a point sink are given in Sect. 4. A brief discussion concludes the paper in Sect. 5.

2 Heuristic results for impulsive start

In this section, we review models for small-time behaviour of a sink that is started impulsively in a fluid with a free surface. Although the derivations are heuristic, they nevertheless reveal some aspects of the analytical structure of the solution at small times, at least for small sink withdrawal strength.

The governing equations for this canonical nonlinear free-surface problem are well known. In this section, they will be discussed for the case of planar flow into a line sink. The fluid is incompressible and inviscid, so that it flows irrotationally. The velocity vector $\mathbf{q} = u\mathbf{e_x} + v\mathbf{e_y}$ can therefore be expressed in terms of a single scalar potential Φ according to the relation $\mathbf{q} = \nabla\Phi$. The velocity potential Φ satisfies Laplace's equation

$$\nabla^2\Phi = 0. \tag{2.1}$$

The fluid is unbounded, and assumed to occupy the lower half-plane $y < 0$ initially. A line sink is located at the point $(x, y) = (0, -h)$ within the fluid, so that the velocity potential there has the singular limiting behaviour

$$\Phi \to -\frac{m}{2\pi} H(t) \log\sqrt{x^2 + (y+h)^2} \quad \text{as } (x, y) \to (0, -h). \tag{2.2}$$

The constant m is the sink strength (fluid volume per time per width along the line sink), and $H(t)$ represents the Heaviside unit step function, which is zero for $t < 0$ and one for $t > 0$. (Strictly, dimensional quantities should not be used in the argument of the logarithm, but this representation simplifies the algebra, and in any event does not affect the outcome since only derivatives of the velocity potential are required).

If the interface has the representation $y = \eta(x, t)$, then the kinematic condition there becomes

$$\frac{\partial\eta}{\partial t} + u\frac{\partial\eta}{\partial x} = v, \tag{2.3}$$

representing the fact that the fluid is not free to cross its own boundary. There is also a dynamic free-surface condition

$$\frac{\partial\Phi}{\partial t} + \frac{1}{2}\left(u^2 + v^2\right) + g\eta = 0 \tag{2.4}$$

on the free surface. Here, g is the downward acceleration of gravity, and the condition comes from Bernoulli's equation in the fluid and the fact that pressure must be constant on the surface. There is, in fact, an ambiguity in the

definition of the velocity potential Φ, since it is only known to an arbitrary additive function of time, so that the constant 0 on the right-hand side of Eq. 2.4 can then be replaced with a function of time, without altering the actual velocity components u and v.

The condition (2.2) corresponds to the sink being turned on impulsively at time $t = 0$, and in that case, there is a heuristic expectation that the velocity potential Φ and surface elevation η should have the small-time behaviour

$$\begin{aligned} \Phi(x, y, t) &= H(t)\left[\Phi_0(x, y) + t\Phi_1(x, y) + t^2\Phi_2(x, y) + \cdots\right] \\ \eta(x, t) &= H(t)\left[t\eta_1(x) + t^2\eta_2(x) + \cdots\right]. \end{aligned} \tag{2.5}$$

These expressions are then substituted in the boundary conditions (2.3) and (2.4) and terms collected at each power of t.

There is, of course, an immediate difficulty with using expressions such as (2.5) in the dynamic free-surface condition (2.4). Since the velocity potential Φ involves the discontinuous Heaviside step function $H(t)$, its time derivative can be expected to give rise to the Dirac delta function $\delta(t)$, which is a generalized function rather than a function in the usual sense (see [16, p. 10]). The difficulty appears at the zeroth power in time, which formally gives the condition

$$\delta(t)\Phi_0 + H(t)\Phi_1 + \tfrac{1}{2}H(t)\left[(\Phi_0)_x^2 + (\Phi_0)_y^2\right] = 0 \quad \text{on } y = 0, \tag{2.6}$$

from the dynamical condition (2.4). In order for this purely heuristic approach to the impulsively started sink problem to continue, it is necessary to interpret this condition (2.6) in a sensible way.

The simplest interpretation of (2.6) is just to demand that

$$\Phi_0(x, 0) = 0, \tag{2.7}$$

and this is effectively the approach taken by Tyvand [8], for example. It is equivalent to imposing zero velocity potential on the undisturbed free surface $\eta = 0$ at time $t = 0$.

With this resolution of the difficulty posed by Eq. 2.6, the heuristic solution now proceeds without further complication. The zeroth-order function Φ_0 satisfies Laplace's equation (2.1) subject to (2.7) on $y = 0$, and the singular condition (2.2) (although with the Heaviside function $H(t)$ deleted). The kinematic condition (2.3) then gives the first-order surface elevation $\eta_1(x)$ from the equation

$$\eta_1(x) = (\Phi_0)_y(x, 0). \tag{2.8}$$

When the zeroth-order velocity potential is obtained in this way, and combined with (2.8) and the expansions (2.5), the potential at small time is found to be

$$\Phi(x, y, t) = -\frac{m}{2\pi}H(t)\left[\log\sqrt{x^2 + (y + h)^2} - \log\sqrt{x^2 + (y - h)^2}\right] \tag{2.9}$$

and the corresponding surface elevation is

$$\eta(x, t) = -H(t)t\frac{mh}{\pi\left(x^2 + h^2\right)}. \tag{2.10}$$

Equation 2.9 shows that the initial potential behaves as if an image source were present above the interface. The surface elevation (2.10) for small times then varies directly with the sink strength m.

Other interpretations of the formal condition (2.6) are also possible, however. In particular, if it is considered that a steady flow into the sink has already been established in the presence of a rigid lid on $y = 0$ which is then impulsively removed at $t = 0$, it is possible simply to take the zeroth-order velocity potential in the form

$$\Phi_0(x, y) = -\frac{m}{2\pi}\left[\log\sqrt{x^2 + (y + h)^2} + \log\sqrt{x^2 + (y - h)^2}\right], \tag{2.11}$$

which is equivalent to an image line sink being present above the fluid. (For an established flow, the potential (2.11) should strictly not be multiplied by the Heaviside function $H(t)$ in Eq. 2.5, although the analysis is unaffected

as this is just a solution to Laplace's equation). The first-order term η_1 for the surface elevation is obtained from Eq. 2.8, and becomes simply

$$\eta_1(x) = 0, \tag{2.12}$$

in view of (2.11).

From (2.5), it is then necessary to consider the first-order term

$$H(t)t\Phi_1(x,0) = -H(t)\frac{tm^2x^2}{2\pi^2\left(x^2+h^2\right)^2},$$

which follows from (2.6) and (2.11), and the identity $t\delta(t) = 0$. The first-order term Φ_1 for the velocity potential may therefore be found by solving Laplace's equation (2.1) in $y < 0$, subject to

$$\Phi_1 = -\frac{m^2x^2}{2\pi^2\left(x^2+h^2\right)^2} \tag{2.13}$$

on the line $y = 0$. Fourier transforms yield the result

$$\Phi_1(x,y) = \frac{m^2}{4\pi^2 h}\frac{x^2(y-2h)+y(y-h)^2}{\left[x^2+(y-h)^2\right]^2}. \tag{2.14}$$

The kinematic condition (2.3) and the expansion (2.5) give the second-order expression

$$\eta_2(x) = (\Phi_1)_y(x,0), \tag{2.15}$$

from which the surface elevation at small time may be calculated, using the solution (2.14). When (2.12) and (2.15) are thus combined with the expansion (2.5), the free surface is found to have the behaviour

$$\eta(x,t) = H(t)t^2\frac{m^2\left[x^4-6x^2h^2+h^4\right]}{4\pi^2 h\left[x^2+h^2\right]^3}. \tag{2.16}$$

This result (2.16) is the same as that obtained by Stokes et al. [14, their Eq. 22], and it shows that the surface elevation varies with the square of the sink strength. It therefore gives a much smaller deformation to the surface, for weak sinks, than the expression (2.10).

These results (2.9–2.11), (2.14), (2.16) have been obtained in an heuristic fashion only, relying on certain interpretations of equations involving discontinuous functions and their derivatives (generalized functions). As such, they can rightly be criticized for their lack of rigour. For this reason, it is appropriate now to investigate linearized theories in more detail, incorporating the effects both of a pre-existent steady-state flow and a time-dependent change to the sink strength. This is done in the next two sections, for planar and axi-symmetric flows, respectively.

3 Linearized analysis for planar flow

The equations of planar flow into a line sink at $(0,-h)$ are the same as given in Sect. 2, except that we choose to replace (2.2) with the expression

$$\Phi \to -\frac{m}{2\pi}G_a(t)\log\sqrt{x^2+(y+h)^2} \quad \text{as } (x,y)\to(0,-h). \tag{3.1}$$

The function $G_a(t)$ in (3.1) is chosen to allow for the case of a steady flow for times $t < 0$, a linear ramp-up of sink strength over time interval $0 < t < a$ and then a final constant strength for $t > a$. Thus we have chosen

$$G_a(t) = \begin{cases} \Delta, & \text{for } t < 0 \\ \Delta + (1-\Delta)t/a, & \text{for } 0 < t < a \\ 1, & \text{for } t > a. \end{cases} \tag{3.2}$$

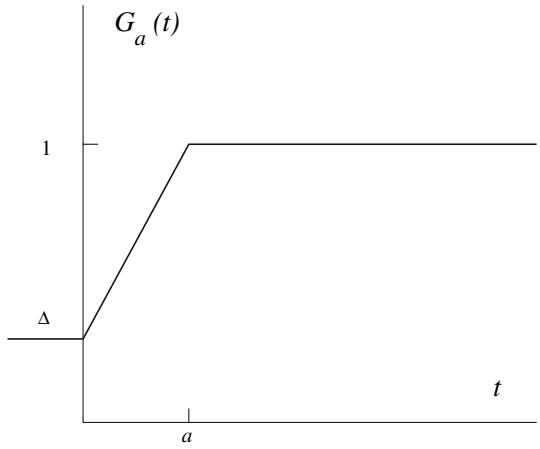

Fig. 1 A sketch of the sink strength function $G_a(t)$

The constant Δ is a dimensionless multiple of the sink strength. For convenience, the function (3.2) is sketched in Fig. 1 . Equation 3.2 represents the simplest continuous function that satisfies the desired criteria of this section; we have also carried out the analysis for other more complicated functions, including a cubic-spline in which $G_a(t)$ and its first two derivatives are continuous, but the results are not significantly altered. For simplicity, therefore, only the case (3.2) will be discussed here. (A similar function is mentioned briefly by Xue and Yue [12]).

We now perform a standard perturbation analysis in powers of the sink strength m (rather than the time t as in Sect. 2). The velocity potential Φ and surface elevation η are represented as

$$\Phi(x, y, t) = m\Phi_1(x, y, t) + \mathcal{O}(m^2), \quad \eta(x, t) = m\eta_1(x, t) + \mathcal{O}(m^2). \tag{3.3}$$

(Strictly, these ought to be expansions in a Froude number, which is the sink strength m made dimensionless using the acceleration g of gravity and the submergence depth h, but this does not affect the analysis). The first-order functions Φ_1 and η_1 satisfy the linearized system of equations

$$\nabla^2\Phi_1 = 0 \tag{3.4}$$

in the lower half-plane $y < 0$ and

$$\Phi_1 \to -\frac{1}{2\pi}G_a(t)\log\sqrt{x^2 + (y+h)^2} \tag{3.5}$$

near the sink at $(0, -h)$, subject to the kinematic condition

$$\frac{\partial\eta_1}{\partial t} = \frac{\partial\Phi_1}{\partial y} \tag{3.6}$$

and the dynamic condition

$$\frac{\partial\Phi_1}{\partial t} + g\eta_1 = 0 \tag{3.7}$$

on the line $y = 0$.

The first-order velocity potential function Φ_1 satisfying the linearized system (3.4)–(3.7) is split into a steady and an unsteady component,

$$\Phi_1(x, y, t) = \Phi_1^S(x, y) + \Phi_1^U(x, y, t),$$

from which it is easily found that

$$\Phi_1^S(x, y) = -\frac{\Delta}{2\pi}\left[\log\sqrt{x^2 + (y+h)^2} + \log\sqrt{x^2 + (y-h)^2}\right]. \tag{3.8}$$

The unsteady component Φ_1^U must be calculated using a combination of Laplace transforms in t and Fourier transforms in x. The process is straighforward, if lengthy, and the final result, when combined with the steady component (3.8) and the expansion (3.3), gives the linearized velocity potential

$$\Phi(x,y,t) = -\frac{m}{2\pi}G_a(t)\log\sqrt{x^2+(y+h)^2} + \frac{m}{2\pi}\left[G_a(t)-2\Delta\right]\log\sqrt{x^2+(y-h)^2} + \frac{m(1-\Delta)}{\pi}\int_0^\infty \mathrm{e}^{\kappa(y-h)}\cos(\kappa x)\left[f(\kappa,t)-H(t-a)f(\kappa,t-a)\right]\mathrm{d}\kappa + \mathcal{O}(m^2). \tag{3.9}$$

Here, it is convenient to define the intermediate function

$$f(\kappa,t) = \frac{t}{a\kappa} - \frac{\sin(\sqrt{\kappa g}t)}{a\kappa\sqrt{\kappa g}},$$

and $H(t-a)$ denotes the Heaviside step function that is zero for $t < a$ and one for $t > a$. The first-order surface height is then obtained from Eq. 3.9 and the dynamic condition (3.7) in the form

$$\eta(x,t) = -\frac{m(1-\Delta)}{\pi g}\int_0^\infty \mathrm{e}^{-\kappa h}\cos(\kappa x)\left[f'(\kappa,t)-H(t-a)f'(\kappa,t-a)\right]\mathrm{d}\kappa + \mathcal{O}(m^2), \tag{3.10}$$

with intermediate function

$$f'(\kappa,t) = \frac{1}{a\kappa} - \frac{\cos(\sqrt{\kappa g}t)}{a\kappa}.$$

A result equivalent to the potential (3.9) is given in complex form by Wehausen and Laitone [17, p. 495].

3.1 Small-time asymptotics

The behaviour of the linearized solution near $t = 0$ is obtained from (3.9) and (3.10) using straightforward Taylor-series expansions of the intermediate functions f and f' in time. (The terms involving the Heaviside function $H(t-a)$ vanish). The coefficients of each power in time are Fourier-cosine transforms that can be evaluated in closed form. For small time, the velocity potential (3.9) behaves as

$$\Phi(x,y,t) \sim \frac{m}{2\pi}\left[-\Delta-(1-\Delta)t/a\right]\log\sqrt{x^2+(y+h)^2} + \frac{m}{2\pi}\left[-\Delta+(1-\Delta)t/a\right]\log\sqrt{x^2+(y-h)^2} - \frac{m(1-\Delta)}{\pi a}\left[\frac{gt^3}{3!}\frac{(y-h)}{x^2+(y-h)^2} + \frac{g^2t^5}{5!}\frac{(y-h)^2-x^2}{\left[x^2+(y-h)^2\right]^2} + \mathcal{O}(t^7)\right] + \mathcal{O}(m^2). \tag{3.11}$$

A case of interest is the limit $\Delta \to 0$, where there is no pre-existing steady flow; the fluid starts from rest at $t = 0$ and the sink ramps up linearly to its final strength m at time $t = a$. The initial flow is then equivalent to a submerged sink and an image line source above the fluid. This is as anticipated by Tyvand [8, Eq. 9] and summarized in Eq. 2.9. When the sink is turned on from an existing steady flow $0 < \Delta < 1$, however, the small-time potential acts like a submerged sink at $(0,-h)$ with either a source or a sink at the image point $(0,h)$, as expected.

The surface elevation η in (3.10) may similarly be analyzed to give its behaviour at small time. Taylor series expansion gives

$$\eta(x,t) \sim -\frac{m(1-\Delta)}{\pi g a}\left[\frac{gt^2}{2!}\frac{h}{x^2+h^2} - \frac{g^2t^4}{4!}\frac{h^2-x^2}{\left[x^2+h^2\right]^2} + \mathcal{O}(t^6)\right] + \mathcal{O}(m^2). \tag{3.12}$$

The first term in this expansion has behaviour similar to that in (2.10).

It is interesting to investigate the behaviour of the linearized interface (3.10) in the limit $a \to 0$ corresponding to instantaneous start of the sink. In this fully impulsive limit, Eq. (3.10) becomes

$$\eta(x,t) \to -\frac{m(1-\Delta)}{\pi}\int_0^\infty \mathrm{e}^{-\kappa h}\cos(\kappa x)\frac{\sin\left(\sqrt{g\kappa}t\right)}{\sqrt{g\kappa}}\mathrm{d}\kappa + \mathcal{O}(m^2), \qquad \text{as } a \to 0. \tag{3.13}$$

A Taylor-series expansion in time may likewise be performed on Eq. 3.13, and each of the coefficients of the powers of t is a Fourier-cosine transform that can be evaluated exactly. The result to third order is

$$\eta(x,t) \sim \frac{m(1-\Delta)}{\pi}\left[-t\frac{h}{x^2+h^2} + \frac{t^3g}{6}\frac{h^2-x^2}{\left[x^2+h^2\right]^2} + \mathcal{O}(t^5)\right] + \mathcal{O}(m^2). \tag{3.14}$$

The two terms in (3.14) are identical to the terms at order t and t^3 in Tyvand [8, Eq. 29], after allowance is made for the non-dimensionalization used in that paper. However, the Tyvand [8] expression also contains a term at order t^2 which is not present in Eq. 3.14; this is due to the effects of nonlinearity, which are not considered in the present analysis.

3.2 Large-time asymptotics

For $t > a$, the function $G_a(t)$ in (3.2) and the Heaviside step function $H(t-a)$ in (3.9) both take the value one, so that the potential may be written

$$\Phi(x,y,t) = -\frac{m}{2\pi}\log\sqrt{x^2+(y+h)^2} + \frac{m(1-2\Delta)}{2\pi}\log\sqrt{x^2+(y-h)^2} + \frac{m(1-\Delta)}{\pi}\int_0^\infty \mathrm{e}^{\kappa(y-h)}\cos(\kappa x)\left[\frac{a\sqrt{\kappa g}-2\sin\left(a\sqrt{\kappa g}/2\right)\cos\left(\sqrt{\kappa g}(t-a/2)\right)}{a\kappa\sqrt{\kappa g}}\right]\mathrm{d}\kappa + \mathcal{O}(m^2). \tag{3.15}$$

To study the behaviour of (3.15) for large time, it is convenient to consider the y-derivative, which may be expressed in the form

$$\frac{\partial\Phi}{\partial y} = -\frac{m}{2\pi}\left[\frac{(y+h)}{x^2+(y+h)^2}+\frac{(y-h)}{x^2+(y-h)^2}\right] - \frac{m(1-\Delta)}{\pi}\int_0^\infty \mathrm{e}^{\kappa(y-h)}\cos(\kappa x)\frac{\sin\left(a\sqrt{\kappa g}/2\right)}{a\sqrt{\kappa g}/2}\cos\left(\sqrt{\kappa g}(t-a/2)\right)\mathrm{d}\kappa + \mathcal{O}(m^2). \tag{3.16}$$

The solution (3.16) is now evaluated along rays $x = ct$, and the trigonometric identity

$$\cos(\kappa x)\cos\left(\sqrt{\kappa g}(t-a/2)\right) = \tfrac{1}{2}\Re\mathfrak{e}\left[\mathrm{e}^{\mathrm{i}tp_1(\kappa)}+\mathrm{e}^{\mathrm{i}tp_2(\kappa)}\right]\mathrm{e}^{-\mathrm{i}a\sqrt{\kappa g}/2}$$

is used, in which it is convenient to define the two functions

$$p_1(\kappa) = \sqrt{\kappa g}+\kappa c, \quad p_2(\kappa) = \sqrt{\kappa g}-\kappa c. \tag{3.17}$$

The method of stationary phase may now be used to give the large-time behaviour of the vertical velocity component in Eq. 3.16. This result is given in [18, p. 371], for example. For an integral of the form

$$I(t) = \int_A^B \mathrm{e}^{\mathrm{i}tp(\kappa)}G(\kappa)\,\mathrm{d}\kappa \tag{3.18a}$$

in which t is a large real parameter and the contour AB lies along the real axis, the function I has the asymptotic form

$$I(t) \sim G(\kappa_0)\mathrm{e}^{\mathrm{i}tp(\kappa_0)}\sqrt{\frac{2\pi}{-tp''(\kappa_0)}}\mathrm{e}^{-\mathrm{i}\pi/4}. \tag{3.18b}$$

Here, κ_0 is a real stationary-phase point $A < \kappa_0 < B$ at which $p'(\kappa_0) = 0$ and $p''(\kappa_0) < 0$.

The function $p_2(\kappa)$ is the only quantity in (3.17) that has a positive stationary phase point, at $\kappa_0 = g/(4c^2)$. The method of stationary phase (3.18) therefore gives the large-time behaviour of (3.16) in the form

$$\frac{\partial\Phi}{\partial y} \sim -\frac{m}{2\pi}\left[\frac{(y+h)}{x^2+(y+h)^2}+\frac{(y-h)}{x^2+(y-h)^2}\right] - \frac{2m(1-\Delta)}{a\sqrt{\pi g t c}}\exp\left(\frac{g(y-h)}{4c^2}\right)\sin\left(\frac{ag}{4c}\right)\cos\left(\frac{g(t-a)}{4c}-\frac{\pi}{4}\right)+\mathcal{O}(m^2). \tag{3.19}$$

Finally, the substitution $c = x/t$ is re-introduced into (3.19), and the result is integrated with respect to y. After a little algebra, the final asymptotic form is obtained for the linearized velocity potential in the form

$$\Phi(x, y, t) \sim -\frac{m}{2\pi}\left[\log\sqrt{x^2+(y+h)^2} + \log\sqrt{x^2+(y-h)^2}\right] - \frac{8m(1-\Delta)}{at^2}\sqrt{\frac{x^3}{\pi g^3}}\exp\left(\frac{gt^2(y-h)}{4x^2}\right)\sin\left(\frac{agt}{4x}\right)\cos\left(\frac{gt(t-a)}{4x}-\frac{\pi}{4}\right)+\mathcal{O}(m^2), \tag{3.20}$$

valid for large time t.

The similar stationary-phase analysis may be applied to the formula (3.10) for the surface elevation. We state the result here, for completeness. For large t,

$$\eta(x,t) \sim -\frac{4m(1-\Delta)}{at}\sqrt{\frac{x}{\pi g^3}}\exp\left(-\frac{ght^2}{4x^2}\right)\sin\left(\frac{agt}{4x}\right)\sin\left(\frac{gt(t-a)}{4x}-\frac{\pi}{4}\right)+\mathcal{O}(m^2). \tag{3.21}$$

The formula (3.20) shows that the velocity potential Φ at large times behaves like a submerged sink, with an image sink above the fluid region. This is the behaviour obtained in Eq. 2.11, using an heuristic argument. This is, of course, to be expected, as the linearized solution must ultimately tend to the steady-state behaviour for large-enough time. However, Eq. 3.20 shows that this behaviour is established exponentially rapidly (since $y < 0$). The surface elevation η in (3.21) vanishes exponentially quickly, at the first order in m, so that the smaller $\mathcal{O}(m^2)$ surface height is attained very rapidly after the sink reaches its steady-state strength, consistently with (2.16).

4 Linearized analysis for axisymmetric flow

We now consider the three-dimensional case, with axi-symmetric flow geometry and an isolated point sink located at $(x, y, z) = (0, 0-h)$. The z-axis now points vertically, and the x- and y-coordinates are directed horizontally. The sink strength M now has dimensions of volume per time.

Linearized equations are derived using a standard perturbation analysis in powers of the sink strength M, similarly to Eq. 3.3. These expansions for the velocity potential Φ and surface elevation η take the form

$$\Phi(x, y, t) = M\Phi_1(x, y, t) + \mathcal{O}(M^2), \quad \eta(x, t) = M\eta_1(x, t) + \mathcal{O}(M^2). \tag{4.1}$$

Cylindrical polar coordinates (r, θ) are defined through the usual relations $x = r\cos\theta$ and $y = r\sin\theta$, and Laplace's equation for the first-order velocity potential function Φ_1 now takes the form

$$\nabla^2\Phi_1 = \frac{\partial^2\Phi_1}{\partial r^2} + \frac{1}{r}\frac{\partial\Phi_1}{\partial r} + \frac{\partial^2\Phi_1}{\partial z^2} = 0. \tag{4.2}$$

Near the sink, the first-order velocity potential has the singular behaviour

$$\Phi_1 \to \frac{1}{4\pi}G_a(t)\frac{1}{\sqrt{r^2+(y+h)^2}} \quad \text{as } (r, z) \to (0, -h). \tag{4.3}$$

Here, the sink strength function $G_a(t)$ is exactly as defined in (3.2) and sketched in Fig. 1. The linearized kinematic and dynamic conditions become

$$\frac{\partial\eta_1}{\partial t} = \frac{\partial\Phi_1}{\partial z} \quad \text{on } z = 0 \tag{4.4}$$

and

$$\frac{\partial\Phi_1}{\partial t} + g\eta_1 = 0 \quad \text{on } z = 0, \tag{4.5}$$

respectively.

In view of the form (4.2) of Laplace's equation for the potential, the solution to the system of equations (4.1)–(4.5) must be obtained using a combination of Laplace transforms in time and Hankel transforms in the radial coordinate r (see, for example, [19]). It is also necessary to make use of the well-known identity [19, p. 219]

$$\int_0^\infty \mathrm{e}^{-h\kappa} J_0(\kappa r)\,\mathrm{d}\kappa = \frac{1}{\sqrt{r^2+h^2}},$$

in which J_0 denotes the first-kind Bessel function of order zero. The calculation is then straightforward and, after some algebra, the velocity potential is obtained in the form

$$\Phi(r,z,t) = \frac{M}{4\pi} G_a(t) \left[\frac{1}{\sqrt{r^2+(z+h)^2}} + \frac{1}{\sqrt{r^2+(z-h)^2}} \right] - \frac{M(1-\Delta)}{2\pi a} \int_0^\infty [f_1(\kappa,t) - H(t-a) f_1(\kappa, t-a)]\, \mathrm{e}^{\kappa(z-h)} J_0(\kappa r)\,\mathrm{d}\kappa + \mathcal{O}(M^2), \tag{4.6}$$

with intermediate function

$$f_1(\kappa,t) = \frac{\sin(\sqrt{g\kappa}\,t)}{\sqrt{g\kappa}}.$$

Again, the symbol $H(t-a)$ represents the Heaviside step function that is zero for $t < a$ and one for $t > a$. The linearized surface height is also found using Laplace and Hankel transforms and may be shown to be

$$\eta(r,t) = -\frac{M(1-\Delta)}{2\pi a g} \int_0^\infty [f_2(\kappa,t) - H(t-a) f_2(\kappa,t-a)]\, \mathrm{e}^{-\kappa h} J_0(\kappa r)\,\mathrm{d}\kappa + \mathcal{O}(M^2), \tag{4.7}$$

with intermediate function

$$f_2(\kappa,t) = 1 - \cos(\sqrt{g\kappa}\,t).$$

When the limit $a \to 0$ is taken in (4.6) and (4.7), in the same way as indicated for (3.13) in the previous section, and the parameter Δ is set to zero, it may be shown that the resulting expressions are identical to those presented by Xue and Yue [12]. An equivalent alternative representation of the potential (4.6) may also be derived from the expression in [17, p. 492].

4.1 Small-time asymptotics

The behaviour of the linearized solution for small times is again obtained by Taylor-series of Eqs. 4.6 and 4.7 in time, in which the terms involving the Heaviside step function $H(t-a)$ all vanish. The coefficients of each power in time are Hankel transforms, for which closed form expressions are known (see [19, p. 220]). After some algebra, the small-time expansion of the velocity potential (4.6) becomes

$$\Phi(r,z,t) \sim \frac{M}{2\pi}[\Delta + (1-\Delta)t/a] \frac{1}{\sqrt{r^2+(z+h)^2}} + \frac{M}{4\pi}[\Delta - (1-\Delta)t/a] \frac{1}{\sqrt{r^2+(z-h)^2}} + \frac{M(1-\Delta)gt^3}{12\pi a} \frac{r}{\left[r^2+(z-h)^2\right]^{3/2}} + \mathcal{O}(Mt^5, M^2). \tag{4.8}$$

For small Δ, when there is no established steady-state flow at $t = 0$, the potential again behaves as if an image source is present above the plane $z = 0$, at least for small times. A similar analysis can be performed for the surface elevation η in (4.7), but yields no new information.

4.2 Large-time asymptotics

For $t > a$, the functions $G_a(t)$ and $H(t-a)$ are both one, and so the velocity potential in (4.6) can be written in the form

$$\Phi(r,z,t) = \frac{M}{4\pi}\left[\frac{1}{\sqrt{r^2+(z+h)^2}} + \frac{1}{\sqrt{r^2+(z-h)^2}}\right] - \frac{M(1-\Delta)}{\pi a}\int_0^\infty \left[\frac{\sin(\sqrt{g\kappa}a/2)\cos\left(\sqrt{g\kappa}(t-a/2)\right)}{\sqrt{g\kappa}}\right] \mathrm{e}^{\kappa(z-h)} J_0(\kappa r)\,\mathrm{d}\kappa + \mathcal{O}(M^2). \tag{4.9}$$

Similarly, the surface elevation becomes

$$\eta(r,t) = -\frac{M(1-\Delta)}{\pi a g}\int_0^\infty \sin(\sqrt{g\kappa}a/2)\sin\left(\sqrt{g\kappa}(t-a/2)\right)\mathrm{e}^{-\kappa h} J_0(\kappa r)\,\mathrm{d}\kappa + \mathcal{O}(M^2). \tag{4.10}$$

In order to study the large-time behaviour of (4.9) and (4.10), we make use of the integral identity for the Bessel function

$$J_0(\kappa r) = \frac{1}{\pi}\int_0^\pi \cos(\kappa r \sin\theta)\,\mathrm{d}\theta,$$

which may be found in [19, p. 212] or [20, p. 360], for example. As in Sect. 3, we again consider the solution along rays $r = ct$, and making use of the above identity, the potential (4.9) becomes

$$\Phi(r,z,t) = \frac{M}{4\pi}\left[\frac{1}{\sqrt{r^2+(z+h)^2}} + \frac{1}{\sqrt{r^2+(z-h)^2}}\right] - \frac{M(1-\Delta)}{2\pi^2 a}\Re\mathfrak{e}\int_0^\pi\int_0^\infty \frac{\sin(\sqrt{g\kappa}a/2)}{\sqrt{g\kappa}}\mathrm{e}^{\kappa(z-h)} \times \mathrm{e}^{-\mathrm{i}a\sqrt{g\kappa}/2}\left[\mathrm{e}^{\mathrm{i}tp_1(\kappa;\theta)} + \mathrm{e}^{\mathrm{i}tp_2(\kappa;\theta)}\right]\mathrm{d}\kappa\,\mathrm{d}\theta + \mathcal{O}(M^2) \tag{4.11}$$

and the surface elevation (4.10) may similarly be expressed as

$$\eta(r,t) = -\frac{M(1-\Delta)}{2\pi^2 a g}\Im\mathfrak{m}\int_0^\pi\int_0^\infty \sin(\sqrt{g\kappa}a/2)\mathrm{e}^{-\kappa h} \times \mathrm{e}^{-\mathrm{i}a\sqrt{g\kappa}/2}\left[\mathrm{e}^{\mathrm{i}tp_1(\kappa;\theta)} + \mathrm{e}^{\mathrm{i}tp_2(\kappa;\theta)}\right]\mathrm{d}\kappa\,\mathrm{d}\theta + \mathcal{O}(M^2). \tag{4.12}$$

The two intermediate functions in these expressions (4.11) and (4.12) are defined as

$$p_1(\kappa;\theta) = \sqrt{g\kappa} + \kappa c\sin\theta, \quad p_2(\kappa;\theta) = \sqrt{g\kappa} - \kappa c\sin\theta. \tag{4.13}$$

The method of stationary phase can now be applied to the inner integrals of these functions (4.11) and (4.12). Only the second function p_2 in (4.13) has a stationary point for positive κ, at fixed θ, at the value $\kappa_0 = g/(4c^2\sin^2\theta)$. By making use of equations (3.18), the potential (4.11) has the large-time asymptotic form

$$\Phi(r,z,t) \sim \frac{M}{4\pi}\left[\frac{1}{\sqrt{r^2+(z+h)^2}} + \frac{1}{\sqrt{r^2+(z-h)^2}}\right] - \frac{M(1-\Delta)}{a}\Re\mathfrak{e}\int_0^\pi \mathrm{e}^{\mathrm{i}tF(\theta)}\sin\left[\frac{ga}{4c\sin\theta}\right] \times \exp\left[\frac{g(z-h)}{4c^2\sin^2\theta}\right]\exp\left[\frac{\mathrm{i}ga}{4c\sin\theta}\right]\frac{\mathrm{e}^{\mathrm{i}\pi/4}}{\sqrt{\pi^3 gtc\sin\theta}}\,\mathrm{d}\theta + \mathcal{O}(M^2). \tag{4.14}$$

In a similar fashion, the surface elevation η in (4.12) becomes, for large time,

$$\eta(r,t) \sim \frac{M(1-\Delta)}{2a}\Im\mathfrak{m}\int_0^\pi \mathrm{e}^{\mathrm{i}tF(\theta)}\sin\left[\frac{ga}{4c\sin\theta}\right]\exp\left[-\frac{gh}{4c^2\sin^2\theta}\right] \times \exp\left[\frac{\mathrm{i}ga}{4c\sin\theta}\right]\frac{\mathrm{e}^{\mathrm{i}\pi/4}}{\sqrt{\pi^3 gtc^3\sin^3\theta}}\,\mathrm{d}\theta + \mathcal{O}(M^2). \tag{4.15}$$

An intermediate function

$$F(\theta) = -g/(4c\sin\theta)$$

has been defined for convenience.

These expressions (4.14) and (4.15) have been written in a form that allows the method of stationary phase (3.18) to be applied again. There is a further stationary-phase point at $\theta_0 = \pi/2$, so that, when the substitution $c = r/t$ is invoked and (3.18) is used, the final form of the velocity potential (4.14) at large time is

$$\Phi(r,z,t) \sim \frac{M}{4\pi}\left[\frac{1}{\sqrt{r^2+(z+h)^2}} + \frac{1}{\sqrt{r^2+(z-h)^2}}\right] - \frac{2\sqrt{2}M(1-\Delta)}{\pi gat}\cos\left[\frac{gt(a-t)}{4r}\right]\sin\left[\frac{gat}{4r}\right]\exp\left[\frac{gt^2(z-h)}{4r^2}\right] + \mathcal{O}(M^2). \tag{4.16}$$

Similarly, the surface elevation (4.15) behaves as

$$\eta(r,t) \sim \frac{\sqrt{2}M(1-\Delta)}{\pi gar}\sin\left[\frac{gt(a-t)}{4r}\right]\sin\left[\frac{gat}{4r}\right]\exp\left[-\frac{ght^2}{4r^2}\right] + \mathcal{O}(M^2). \tag{4.17}$$

Equation 4.16 shows that the potential Φ approaches the steady-state-type behaviour, with an image sink above the fluid, exponentially rapidly. Likewise, the expression (4.17) decays to zero extremely rapidly after time $t = a$, so that only a small $\mathcal{O}(M^2)$ surface elevation exists.

Figure 2 shows the velocity potential Φ for the axi-symmetric case, as a function of radial distance r. All profiles were evaluated at the linearized surface $z = 0$, for the case $\Delta = 0.1$. This is therefore a case in which a small steady-state flow was already established when the sink strength was increased at $t = 0$. The steady-state potential for eventual sink strength M is indicated with the thicker dotted line on the figure. The three solid lines represent the velocity potential at the three times $t/a = 0$, 4 and 8, computed directly from (4.6) using numerical quadrature. The small contribution to the initial profile $t = 0$ is caused by the pre-existent source flow of strength $M\Delta$. As time increases, the potential rapidly approaches the steady-state profile near $r = 0$, but also forms a wave that moves radially outwards. The dashed line represents the potential evaluated from the asymptotic solution (4.16) at $z = 0$. There is close agreement between this result and the numerically computed profile at $t/a = 8$.

The surface elevation for the same three times is shown in Fig. 3. These were computed by numerical quadrature from (4.7). Numerically produced movies of the interface show that there is a large initial dip in the interface near $r = 0$, which then overshoots before returning asymptotically to zero, to this order $\mathcal{O}(M)$ of accuracy. (The eventual steady-state has an $\mathcal{O}(M^2)$ surface elevation, which is not accessible to this linearized solution). A small train of

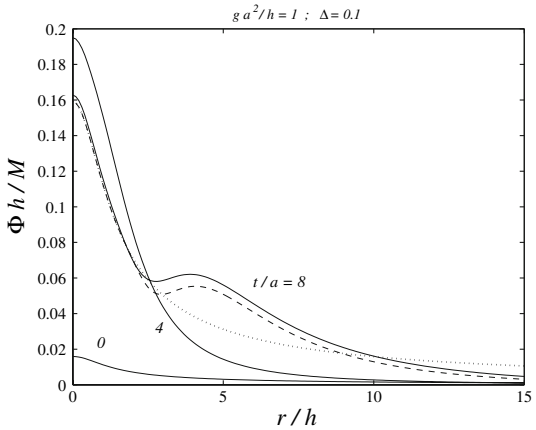

Fig. 2 Velocity potential function Φ (in non-dimensional coordinates) as a function of radial coordinate r/h, at the linearized surface $z = 0$. The three solid lines are the solutions at times $t/a = 0, 4$ and 8, as indicated on the figure. The thicker dotted line is the steady-state solution and the dashed line is the profile predicted by the asymptotic solution (4.16)

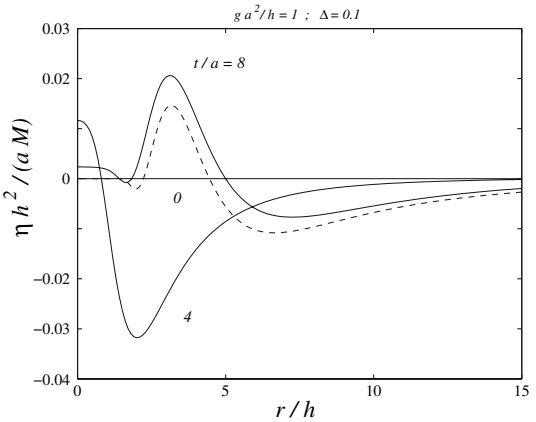

Fig. 3 Surface height η (in non-dimensional coordinates) as a function of radial coordinate r/h. The three solid lines are the solutions at times $t/a = 0, 4$ and 8, as indicated on the figure. The dashed line is the profile predicted by the asymptotic solution (4.17)

transient waves is also seen to move radially outward from the centre, and the first of these is visible in Fig. 3. The dashed line represents the asymptotic solution (4.17) at time $t/a = 8$.

5 Conclusions

This paper has considered the linearized solutions for both two-dimensional planar flow into a submerged line sink in unbounded fluid, and axisymmetric flow into a point sink in three-dimensional flow. In both cases, it has been shown that the analytical structure of the solution at small times is equivalent to an effective image *source* being present above the fluid, as anticipated by the heuristic results (2.9) and (2.10) appropriate for the extreme case in which the sink is started impulsively. The undisturbed surface is the equipotential $\Phi = 0$ in (2.7), as suggested by Tyvand [8]. However, the flow then evolves rapidly toward a situation in which the analytical structure involves an effective image *sink* above the fluid, as for steady flow. Indeed, if a steady-state flow is already present at $t = 0$ when the strength of the sink is increased, an effective image sink is already present above the fluid so that, physically, the flow is more likely to resemble an orderly time-dependent transition from a steady state at one sink strength to a new steady state at increased strength. This corresponds more closely to the situation that exists in practical reservoir management, when demand for water increases smoothly from one level to another.

The analysis presented in this paper has been confined essentially to linearized theories, which assume that the strength of the sink is small. These results are only capable of indicating flow behaviour in the one case in which the flow ultimately evolves to a steady state. In such cases, the predictions of linearized theory are in agreement with nonlinear results, such as those presented by Stokes et al. [14]. In addition, when an initial steady-state flow is already present and the sink strength is increased, the orderly progression from one steady solution to another predicted here is confirmed by these nonlinear results. However, there are two additional nonlinear solution types that are not accessible to this linearized analysis. These involve situations in which the interface itself is drawn into the sink, or else a vertical jet is produced, as discussed by Xue and Yue [12] and Stokes et al. [14]. The fact that these other two types, which exist at higher withdrawal rates, are not available to linearized theories is seen by Xue and Yue [12] as a weakness of such analyses, although numerical simulations appear to be the only options for such highly nonlinear situations.

A question of very great practical interest for unsteady withdrawal models concerns the maximum sink strength for which steady states can be achieved. There is a great disparity between this maximum strength, as computed by Xue and Yue [12] for example, and that computed directly from a steady-state formulation by Forbes and Hocking [4]. We suggest that the discrepancy is likely to be a result of the initial conditions assumed for the unsteady flow simulations, and that impulsively turning the sink on at $t = 0$ is not a good method of maximizing the sink strength for which steady states can be achieved. From the purely mathematical point of view, of course, there is no single "right" initial condition for an unsteady flow, and starting velocity potentials and surface elevations could be selected from an entire function space of such possibilities. However, given the importance of achieving long-term steady withdrawal flows in many practical situations in reservoir management, and so on, the question of designing start-up conditions that allow maximum steady sink strengths to be attained would appear to be an important area for further research in fully nonlinear simulations.

Acknowledgements This work was supported, in part, by Australian Research Council discovery grant DP0450225. Comments from Referees are gratefully acknowledged.

References

1. Tuck EO, Vanden-Broeck J-M (1984) A cusp-like free-surface flow due to a submerged source or sink. J Austral Math Soc, Ser B 25:443–450
2. Hocking GC (1995) Supercritical withdrawal from a two-layer fluid through a line sink. J Fluid Mech 297:37–47
3. Forbes LK, Hocking GC (1993) Flow induced by a line sink in a quiescent fluid with surface tension effects. J Austral Math Soc, Ser B 34:377–391

4. Forbes LK, Hocking GC (1990) Flow caused by a point sink in a fluid having a free surface. J Austral Math Soc, Ser B 32:231–249
5. Vanden-Broeck J-M, Keller JB (1997) An axisymmetric free surface with a 120 degree angle along a circle. J Fluid Mech 342:403–409
6. Forbes LK, Hocking GC (2005) Flow due to a sink near a vertical wall, in infinitely deep fluid. Comput Fluids 34:684–704
7. Lucas SK, Kucera A (1996) A boundary integral method applied to the 3D water coning problem. Phys Fluids 8:3008–3022
8. Tyvand PA (1992) Unsteady free-surface flow due to a line source. Phys Fluids A 4:671–676
9. Sozer EM, Greenberg MD (1995) The time-dependent free surface flow induced by a submerged line source or sink. J Fluid Mech 284:225–237
10. Zhou Q-N, Graebel WP (1990) Axisymmetric draining of a cylindrical tank with a free surface. J Fluid Mech 221:511–532
11. Baek JH, Chung HY (1998) Numerical analysis on axisymmetric draining from a cylindrical tank with a free surface. Comput Fluid Dyn J 6:413–425
12. Xue M, Yue DKP (1998) Nonlinear free-surface flow due to an impulsively started submerged point sink. J Fluid Mech 364:325–347
13. Miloh T, Tyvand PA (1993) Nonlinear transient free-surface flow and dip formation due to a point sink. Phys Fluids A 5:1368–1375
14. Stokes TE, Hocking GC, Forbes LK (2003) Unsteady free-surface flow induced by a line sink. J Eng Math 47:137–160
15. Tyvand PA, Haugen KB (2005) An impulsive bathtub vortex. Phys Fluids 17:062105
16. Lighthill MJ (1980) An introduction to Fourier analysis and generalised functions. Cambridge University Press, Cambridge
17. Wehausen JV, Laitone EV (1960) Surface waves. In: Encyclopaedia of physics, vol 9. Springer Verlag, Berlin
18. Marsden JE (1973) Basic complex analysis. Freeman, San Francisco
19. Andrews GE, Askey R, Roy R (2000) Special functions. Cambridge University Press, Cambridge
20. Abramowitz M, Stegun IA (1972) Handbook of mathematical functions. Dover, New York